Wave Packet Dynamics in the Presence of a Conical Intersection

Paola Cattaneo and Maurizio Persico*

Dipartimento di Chimica e Chimica Industriale, Università di Pisa, v. Risorgimento 35, I-56126 Pisa, Italy

Received: December 4, 1996; In Final Form: February 26, 1997[⊗]

We present a model study of the nonadiabatic wave packet dynamics in the presence of a conical intersection. The wave packet travels essentially along a symmetric coordinate, modeling a photodissociation process, while it is stationary or makes small amplitude vibrations in the coupling modes. We explore the range of applicability of a treatment based on classical trajectories plus surface hopping, comparing it with a full quantum mechanical one. A mixed procedure, classical for the symmetric coordinate and quantum mechanical for the coupling modes, yields very accurate results and allows for a qualitative interpretation of the dynamics. We find that the dynamical behavior of a multidimensional conical intersection can be characterized in terms of a single coupling coordinate, associated with an effective coupling strength parameter.

1. Introduction

The importance of conical intersections in photochemistry, spectroscopy, and collision dynamics has been widely acknowledged in the last years.[1−11] Full quantum mechanical treatments of nonadiabatic wave packet dynamics in two to four dimensions (2D−4D) have been performed.[4,5,9] With particular forms of the vibronic Hamiltonian, more modes can be treated;[12] in general, however, when all the coordinates of more than three atoms are involved, only semiclassical methods[13−17] seem to be viable.

In a previous paper by one of us and other authors,[18] a harmonic (all bound) model of a conical intersection was set up and the two-dimensional (2D) dynamics was examined by means of quantum mechanical and semiclassical surface hopping (TSH) methods. In that study, the initial conditions and the potentials were such that the wave packet went through the conical intersection traveling along the symmetric coordinate, *X*, while it was almost stationary along the antisymmetric (or coupling) coordinate, *Y*. We focused our attention on the transition probability $P_{u\to l}$, from the upper to the lower adiabatic surface, after a single crossing of the near degeneracy region (see Manthe and Köppel[19] and Seidner and Domcke[20] for the study of long-time behaviors). We found that the dynamics remains sustantially diabatic ($P_{u\to l} > 0.8$) in a wide range of coupling strengths. The semiclassical approach correctly reproduces the quantum mechanical results only for weak couplings, whereas it gives lower transition probabilities in the strong coupling regime. A second paper[21] examined a variety of harmonic models (different relationships between starting and crossing points and positions of minima along the *X* coordinate).

In the present work we set up a different model of conical intersection, which is dissociative along the *X* coordinate (section 2.A). Conical intersections standing in a dissociation pathway are found, for instance, in ammonia[9] and in the $C_2H_4^+$ ion.[2] In order to compare the 2D, 3D, and 4D dynamics, we introduce 1, 2, or 3 coupling coordinates (section 4). Quantum mechanical, semiclassical, and mixed treatments of the wave packet dynamics are briefly described in sections 2.B−2.D. The 2D results obtained with a mixed method (section 3) show that, while it is important to treat quantum mechanically the motion along the coupling coordinate *Y*, the classical approach is adequate for the *X* motion. The effect of different initial conditions, with some excitation also in the *Y* mode, is examined in section 3.B. In section 4 we show how the dynamics computed in higher dimensional cases can be understood and approximately predicted on the basis of a 2D model.

2. Model and Theory

2.A. Model Hamiltonian. The 2D model is completely specified by the electronic Hamiltonian matrix **H** in a diabatic basis, as a function of the internal coordinates *X* and *Y*, plus the nuclear kinetic energy operator $\hat{T}_{nuc}$:

$$H_{11}(X,Y) = D_1 e^{-\alpha_1(X+X_1)} + {}^1/_2 KY^2 \tag{1}$$

$$H_{22}(X,Y) = D_2[e^{-2\alpha_2(X-X_2)} - 2e^{-\alpha_2(X-X_2)}] + {}^1/_2 KY^2 + \Delta$$

$$H_{12}(X,Y) = \gamma Y e^{-\beta_1(X-X_3)^2} e^{-\beta_2 Y^2}$$

$$\hat{T}_{nuc} = -\frac{1}{2M_x}\frac{\partial^2}{\partial X^2} - \frac{1}{2M_y}\frac{\partial^2}{\partial Y^2} \tag{2}$$

The derivative couplings (matrix elements of $\partial/\partial Q$ and $\partial^2/\partial Q^2$, where $Q \equiv X,Y$) vanish in the electronically diabatic basis. The parameters of the model take on fixed values (in atomic units):

$$D_1 = 1, \quad D_2 = 0.015, \quad \Delta = 0.015, \quad K = 0.09, \tag{3}$$

$$X_1 = 4, \quad X_2 = 3, \quad X_3 = 6,$$

$$\alpha_1 = 0.4, \quad \alpha_2 = 1, \quad \beta_1 = 0.5, \quad \beta_2 = 1.5,$$

$$M_x = 20\,000, \quad M_y = 10\,000$$

As a consequence, the frequency for the *Y* oscillator is $\omega_y = 0.003$ au $\simeq 658$ cm^{-1}. The only parameter that is varied, in order to test the influence of the coupling strength, is the factor γ in the expression of H_{12}. Diagonalization of the **H** matrix yields the adiabatic energies E_1 and E_2, with a conical intersection for $X \simeq 6.63$, $Y = 0$ bohr. In Figures 1 and 2 we show the diabatic and adiabatic potentials, respectively, and in Figure 3 the electronic coupling H_{12}, for $\gamma = 0.03$ au.

The initial conditions correspond to a sudden Franck−Condon excitation to the H_{11} surface, from a hypothetical ground state harmonic surface with a minimum at $X = 3$, $Y = 0$ bohr, and force constants $K_x = 0.1$, $K_y = 0.09$ au. This yields a Gaussian

* E-mail: mau@hermes.dcci.unipi.it.

[⊗] Abstract published in *Advance ACS Abstracts,* April 15, 1997.

S1089-5639(96)03979-5 CCC: $14.00

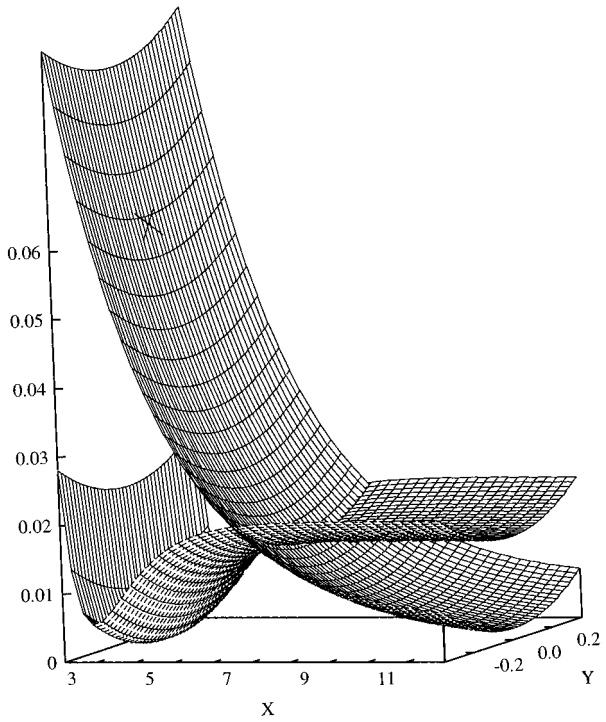

Figure 1. Diabatic potentials H_{II} for the 2D model. Energies and distances in au. The cross marks the center of the initial wave packet.

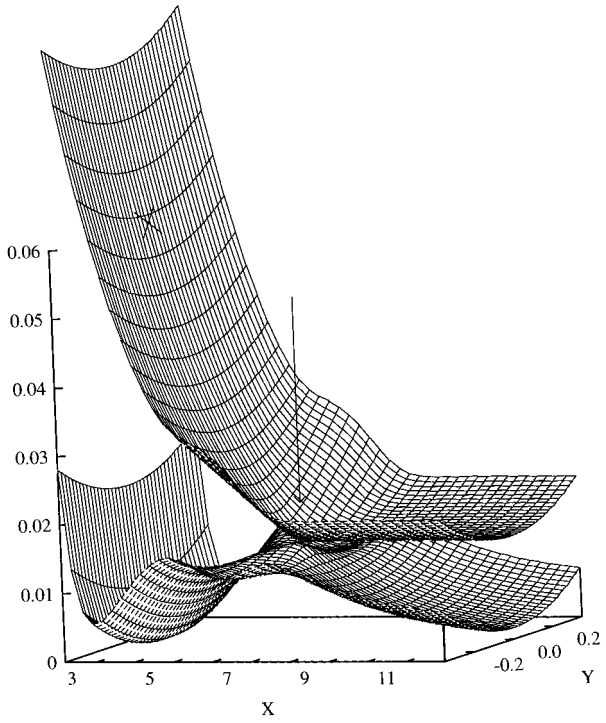

Figure 2. Adiabatic potentials E_K for the 2D model, with coupling factor $\gamma = 0.03$ au. Energies and distances in au. The cross marks the center of the initial wave packet. The arrow indicates the position of the conical intersection.

wave packet with standard deviations $\Delta X = 0.11$ and $\Delta Y = 0.13$ bohr. As the stationary $v = 0$ vibrational state for the Y coordinate is initially populated in the H_{11} potential, we expect almost no evolution of the wave packet in the Y direction, until the coupling region is reached. The wave packet will travel essentially in the X direction, crossing only once the conical intersection. In the Frank−Condon region, as well as in the asymptotic one ($X > 9$ bohr), the adiabatic and diabatic surfaces almost coincide, because $|H_{11} - H_{22}| \gg |H_{12}|$. We have run the quantum mechanical simulations (see below) with slightly different initial conditions, corresponding to the same Gaussian

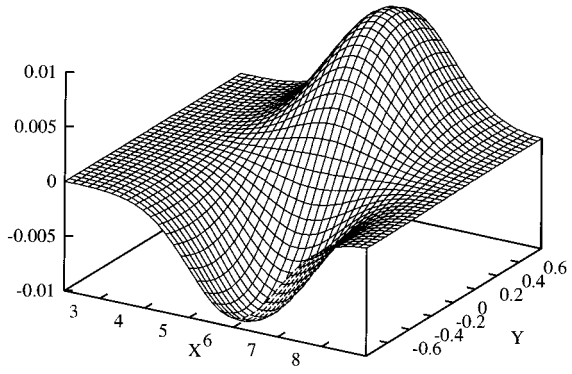

Figure 3. Electronic coupling matrix element between diabatic states, H_{12}, for the 2D model, with coupling factor $\gamma = 0.03$ au. Energies and distances in au.

wave packet in the upper adiabatic surface, instead of the diabatic one: the results are almost identical, with a difference of about 0.01% in the final state probabilities. In section 3.B we shall discuss the results obtained with different, stationary or nonstationary, Y-mode wave functions.

2.B. Quantum Mechanical Wave Packet Propagation. The time-dependent wave function can be written as

$$|\Psi(t)\rangle = \sum_{I=1}^{2} \sum_{v=0}^{v_{max}} \xi_{I,v}(X,t)|I,v\rangle \tag{4}$$

where $|I,v\rangle$ denotes the vth eigenstate of a harmonic oscillator for the Y coordinate, associated with the Ith electronic diabatic state. In this vibronic basis the molecular Hamiltonian takes the form

$$\langle I,v|\hat{H}\,|J,v'\rangle = H^{(V)}_{Iv,Jv'}(X) - \delta_{IJ}\delta_{vv'}\frac{1}{2M_x}\frac{\partial^2}{\partial X^2} \tag{5}$$

The coincidence of equilibrium points ($Y_0 = 0$) and force constants ($K = 0.09$ au) for the two diabatic surfaces makes the treatment based on the expansion (4) particularly simple, if the Y-vibrational basis set is defined with reference to a harmonic oscillator with the same Y_0 and K. Then, the two blocks of the Hamiltonian belonging to the diabatic states 1 and 2 are diagonal, with

$$H^{(V)}_{Iv,Iv}(X) = H_{II}(X,0) + \hbar\omega_y(v + 1/2) \tag{6}$$

The coupling between the diabatic states is contained in the interblock matrix elements:

$$\langle 1,v|\hat{H}\,|2,v'\rangle = H^{(V)}_{1v,2v'}(X) = \int_{-\infty}^{+\infty} H_v(M_y^{1/2}\omega_y^{1/2}Y)H_{v'}(M_y^{1/2}\omega_y^{1/2}Y)\mathrm{e}^{-M_y\omega_y Y^2}H_{12}(X,Y)\,\mathrm{d}Y \tag{7}$$

which can be reduced to a closed form making use of the properties of the Hermite polynomials H_v. Notice that an arbitrary form of the potentials H_{II} and of the coupling H_{12} could be treated with a modest increase in the complexity of the algorithm (see for instance Cimiraglia *et al.*[22]).

The diagonal terms of the vibronic Hamiltonian $\mathbf{H}^{(V)}$ are effective potentials for the nuclear motion in the X coordinate: they are shown in Figure 4. They undergo a set of crossings approximately at the same X of the conical intersection. The $|I,v\rangle$ basis is diabatic, in the sense that it is independent of X and the matrix elements $\langle I,v|\partial/\partial X|J,v'\rangle$ vanish. Diagonalization of the $\mathbf{H}^{(V)}$ matrix yields vibronic adiabatic energies, whereby some of the crossings become avoided.

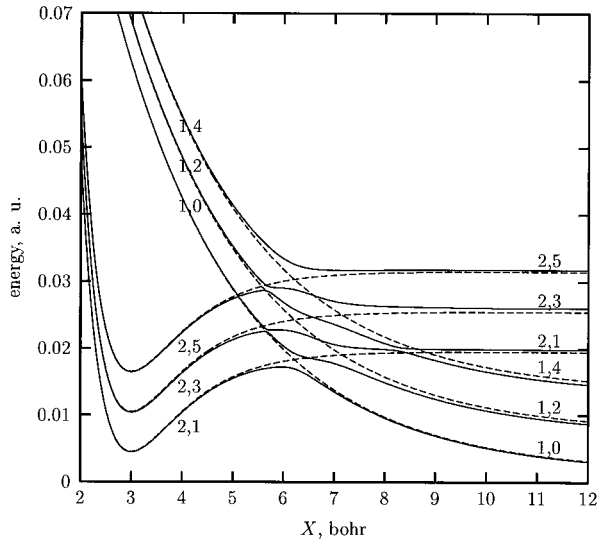

Figure 4. Dashed lines: potential energy curves for the vibronic states $|I,\upsilon\rangle$ ($I \equiv$ electronic diabatic state; $\upsilon \equiv$ vibrational quantum number for the coupling mode Y). Full lines: corresponding eigenvalues (adiabatic potentials). Only one manifold of interacting states is shown: even υ for $I = 1$ and odd υ for $I = 2$.

The multistate nonadiabatic propagation of the $\xi_{I,\upsilon}$ wave packets has been computed by the split-operator fast Fourier transform method, as implemented by Broeckhove *et al.*[23] in the TEMPO package. The population of the vibronic state $|I,\upsilon\rangle$ *is* $P_{I,\upsilon}^{(\mathrm{Q,M})} = \int|\xi_{I,\upsilon}|^2(X)\,\mathrm{d}X$; the total probability for the electronic state I is $P_I^{(\mathrm{QM})} = \sum_\upsilon P_{I,\upsilon}^{(\mathrm{Q,M})}$.

2.C. Mixed Quantal−Semiclassical Treatment Based on the Vibronic Model. The time-evolution problem defined by the X-dependent $\mathbf{H}^{(\mathrm{V})}$ Hamiltonian can be treated in a semiclassical way: we shall call this approach the vibronic model (VM) of the dynamics (see also Ferretti *et al.*[18,21]). In the VM, the classical equations of motion are applied to the X coordinate, while the time-dependent Schrödinger equation is solved for the vibronic wave function:

$$|\Phi(t)\rangle = \sum_{I=1}^{2}\sum_{\upsilon=0}^{\upsilon_{\max}} C_{I,\upsilon}(t)|I,\upsilon\rangle \tag{8}$$

The coefficients $C_{I,\upsilon}(t)$ obey a set of coupled equations:

$$\frac{\partial \mathbf{C}}{\partial t} = -\frac{\mathrm{i}}{\hbar}\mathbf{H}^{(\mathrm{V})}(X(t))\mathbf{C}(t) \tag{9}$$

The $X(t)$ trajectory, for simplicity, has been considered to depend only on the initial diabatic potential, $H_{1,0}(X)$, although a surface-hopping algorithm might be applied to the VM as to the completely semiclassical calculations (see section 2.C). A very accurate solution of the coupled equations (9) can be easily obtained by numerical integration. The square modules of the coefficients are the populations of the vibronic states: $P_{I,\upsilon}^{(\mathrm{VM})} = |C_{I,\upsilon}|^2$; for the electronic states, $P_I^{(\mathrm{VM})} = \sum_\upsilon P_{I,\upsilon}^{(\mathrm{VM})}$.

For a sake of simplicity and of a better qualitative understanding, one can apply the Landau−Zener rule to the avoided crossings between the $H_{I\upsilon,I\upsilon}^{(\mathrm{V})}(X)$ curves, instead of solving directly the coupled equations. For a crossing between states $|I,\upsilon\rangle$ and $|J,\upsilon'\rangle$, the transition probability is

$$P(I,\upsilon \rightarrow J,\upsilon') = 1 - \exp\left[-\frac{2\pi(H_{I\upsilon,J\upsilon'}^{(\mathrm{V})})^2}{\dot{X}F_x}\right] \tag{10}$$

where $\dot{X}$ is the velocity and F_x the slope difference between the $H_{I\upsilon,I\upsilon}^{(\mathrm{V})}$ and $H_{J\upsilon',J\upsilon'}^{(\mathrm{V})}$ potentials; all quantities are evaluated at the crossing point. Notice that, because H_{12} is an odd function of Y, only transitions between states with υ and υ' of different parity are allowed (with both υ and υ' even or odd, $H_{I\upsilon,J\upsilon'}^{(\mathrm{V})} = 0$). This shows that, starting with $\upsilon = 0$ in the electronic state 1, the final wave packets will be an even function of Y in the same electronic state and an odd one in state 2. The final probabilities $P_{I,\upsilon}^{(\mathrm{VM-LZ})}$ of the vibronic states are obtained by applying eq 10 sequentially to all the avoided crossings, within a branching scheme: this will be denoted as the Landau−Zener solution of the vibronic model (VM-LZ). Once more, total electronic probabilities are derived by summing up the vibronic ones: $P_I^{(\mathrm{VM-LZ})} = \sum_\upsilon P_{I,\upsilon}^{(\mathrm{VM-LZ})}$.

A further approximation consists in assuming a linear (nondamped) form for the coupling function, i.e. $H_{12} = \gamma Y$; this may be valid within the initial width of the wave packet (see Figure 3). Then, starting in the $|1,0\rangle$ state, only two crossings are effective in causing transitions: the first one between $|1,0\rangle$ and $|2,0\rangle$, the second between $|2,1\rangle$ and $|1,2\rangle$. The $H_{1\upsilon,2\upsilon'}^{(\mathrm{V})}$ matrix elements take on very simple forms,[18] so that the final probability of being in the diabatic state 1, i.e. the adiabatic transition probability $P_{\mathrm{u}\rightarrow\mathrm{l}}$, is a function of a single parameter λ:

$$P_{\mathrm{u}\rightarrow\mathrm{l}} = P_1^{(\mathrm{VM-SLZ})} = 1 - \mathrm{e}^{-2\lambda} + \mathrm{e}^{-3\lambda} \tag{11}$$

with

$$\lambda = \frac{2\pi\Delta Y^2\gamma^2}{\dot{X}F_x} \tag{12}$$

$\Delta Y = (2M_y\omega_y)^{-1/2}$ is the width of the wave packet. In terms of the adiabatic potentials, γ is the slope of the sides of the double cone along the Y direction: the analogous parameter for the X coordinate is $F_x/2$. Equations 11 and 12 embody what we shall call the simplified Landau−Zener solution of the vibronic model (VM-SLZ). The VM-SLZ results are accurate in a restricted range of γ values (weak coupling), otherwise they are only qualitatively correct, as we shall see in section 3. However, the parameter λ is a good measure of the effective coupling in a much wider range of situations, and it turns out very useful in comparing different conical intersections: we shall express all our results as functions of λ.

2.D. Semiclassical Dynamics: Trajectories plus Surface Hopping. The treatment based on classical trajectories for the nuclear motion and surface hopping to represent electronically nonadiabatic transitions has already been described.[18] We shall give here a brief outline of the algorithm. The time-dependent wave function is expressed as

$$|\psi(t)\rangle = \sum_K A_K(t)\mathrm{e}^{-\mathrm{i}\gamma_K(t)}|\psi_K(\mathbf{Q})\rangle \tag{13}$$

Here $\gamma_K(t) = \int_0^t \mathrm{E_K}(\mathbf{Q})\,\mathrm{d}t$ and the $|\psi_K\rangle$ are the adiabatic states:

$$|\psi_K\rangle = \sum_I C_{IK}|I\rangle \tag{14}$$

with eigenvectors $\boldsymbol{C}_K$ obtained by diagonalization of the $\mathbf{H}$ matrix. The Schrödinger equation for the electrons gives place to a set of coupled equations:

$$\frac{\partial A_K}{\partial t} = -\sum_{L\neq K} A_L(t)\mathrm{e}^{\mathrm{i}(\gamma_K-\gamma_L)}\sum_\alpha \dot{\mathrm{Q}}_\alpha G_{KL}^{(\alpha)} \tag{15}$$

where

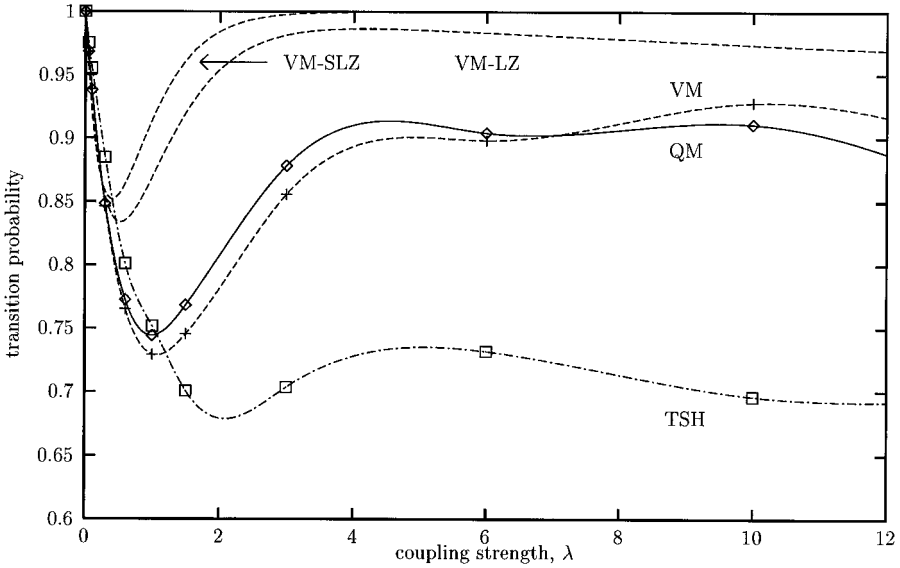

Figure 5. Transition probability from the upper to the lower adiabatic surface, $P_{u\to l}$, for the 2D model, with the initial wave packet corresponding to the $v = 0$ eigenfunction for the coupling mode *Y*.

$$G_{KL}^{(\alpha)} = (E_K - E_L)^{-1}\mathbf{C}_K^{\dagger}\frac{\partial \mathbf{H}}{\partial Q_\alpha}\mathbf{C}_L \qquad (16)$$

The electronic Hamiltonian matrix **H**, its eigenvectors $\boldsymbol{C}_K$, and its eigenvalues E_K are functions of time through the nuclear coordinates ($\boldsymbol{Q} \equiv$ X,*Y* in our model); therefore the integration of eq 15 depends on the trajectory. The classical equations of motion are integrated[29] for a given potential energy surface E_K, and we make use of Tully's fewest switches algorithm[13,14] to introduce surface hoppings to other surfaces, according to changes in the state probabilities $|A_I(t)|^2$. Notice that, within purely quantum mechanical methods, switching from the diabatic to the adiabatic representation is in principle a mere change of basis set, without influence on the computational results; on the contrary, the classical trajectories depend on the definition of the potential, and, according to our experience, the adiabatic surfaces give better results.[24]

We ran a batch of 1000 trajectories with a statistical sampling of initial conditions for each value of the model parameters. The purpose is 2-fold. First, we want to reproduce, as best as possible, the quantum mechanical initial distribution of coordinates and velocities: this is done by sampling independently the four variables *X*, $\dot{X}$, *Y*, and $\dot{Y}$, according to the appropriate Gaussian distributions. The second purpose is to allow for a statistically significant number of random choices in the surface-hopping algorithm. The final probability $P_K^{(TSH)}$ for the electronic state *K* is computed as an average of $|A_K|^2$ over all trajectories.

3. Results of 2D Calculations

3.A. Stationary ($v = 0$) Initial Wave Packet in the Coupling Mode. We present first the results of simulations starting with a Gaussian 2D wave packet, which corresponds to the $|1,0\rangle$ vibronic state, as already described in section 2.A. In Figure 5 we show the final probability for the diabatic state 1, i.e. the transition probability $P_{u\to l}$ from the upper to the lower adiabatic state, obtained for a set of different values of the parameter γ. Actually, we put on the horizontal axis the effective coupling strength λ, which has a more universal meaning than γ; in our model, $\lambda = 8311\gamma^2$.

The quantum mechanical transition probability, $P_1^{(QM)}(\lambda)$, has a minimum value of 0.74 for $\lambda \simeq 1$; the probability goes up to 0.80−0.90 for stronger couplings. The reason for this behavior is clear if one considers the VM-LZ model, or the simplified version, VM-SLZ, which gives qualitatively correct results. For weak couplings all the avoided crossings are close to the diabatic limit, therefore the system will remain in the initial state, $|1,0\rangle$. For strong couplings, the system jumps from $|1,0\rangle$ to $|2,v\rangle$ (mainly $v = 1$, but also higher odd numbers) with a high probability, when the corresponding potentials cross; then, another crossing with the state $|1,v+1\rangle$ causes a second transition, which returns to the initial diabatic electronic surface. For intermediate couplings there is a rather large probability of switching only once the electronic state, from 1 to 2, whence the minimum in $P_{u\to l}(\lambda)$.

The VM results obtained by numerical integration of eq 9 are in excellent agreement with the full quantum mechanical ones. This shows that a classical treatment of large amplitude symmetric modes can be accurate and very effective in reducing the computational burden. The VM-LZ and VM-SLZ solutions deviate from the exact one for moderate to large values of the coupling parameter λ. In fact, the application of the Landau−Zener rule to a multicrossing problem is safe only if the avoided crossing regions do not overlap, which is true in the weak coupling limit. The TSH results also agree with the quantum mechanical ones up to $\lambda = 1$; for larger couplings the semiclassical transition probability is too low. From the comparison of the QM, VM, and TSH results we can conclude that it is important to treat quantum mechanically the motion along the antisymmetric coupling coordinate *Y*. A discussion of this point was already given in Ferretti *et al.*;[18] we add now the conclusive support of the comparison between full QM, VM (*X* mode treated classically), and TSH results (both *X* and *Y* treated classically).

3.B. Vibrational Excitation of the Initial Wave Packet in the Coupling Mode. One may suspect that the partial failure of the semiclassical algorithm is connected with the particular initial wave packet we have chosen, i.e. the eigenfunction $v = 0$ in the antisymmetric coordinate *Y*. With higher v, the ambiguities and shortcomings connected with the classical representation of the zero-point vibration should become less important. Therefore, we have run three sets of calculations with different initial conditions. In the first set, A, instead of $v = 0$ in the *Y* mode, we choose $v = 1$. In the second and third cases, B and C, we have nonstationary wave packets, with the same energy as in A. The initial wave packet B is the $v = 0$ eigenfunction, but centered at $Y = (2\hbar/M_y\omega_y)^{1/2}$. In case C we have again the same Gaussian, centered at $Y = 0$, but multiplied

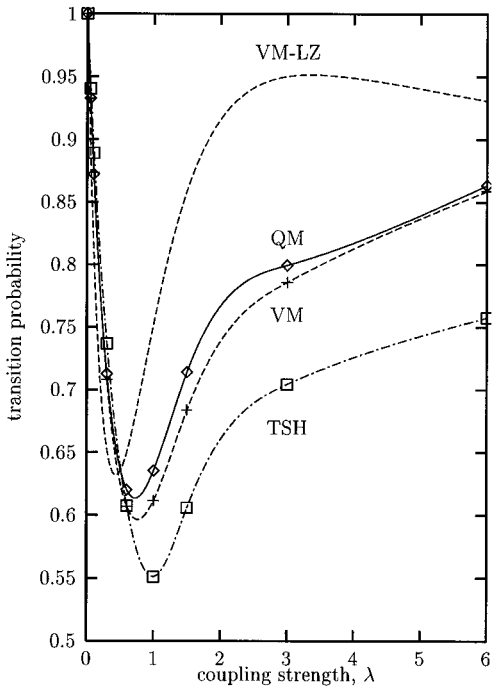

Figure 6. Transition probability from the upper to the lower adiabatic surface, $P_{u\to l}$, for the 2D model, with the initial wave packet corresponding to the $v = 1$ eigenfunction for the coupling mode Y (case A, section 3.B).

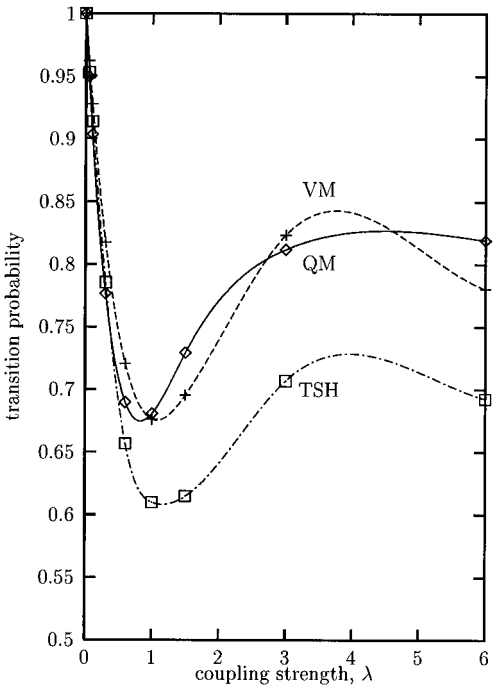

Figure 7. Transition probability from the upper to the lower adiabatic surface, $P_{u\to l}$, for the 2D model. The initial Gaussian wave packet is displaced along the Y coordinate (case B, section 3.B).

by a factor $\exp(i\bar{p}_y Y/\hbar)$, that is, with an average momentum $\bar{p}_y = (2M_y\hbar\omega_y)^{1/2}$. In practice, B and C are two wave packets oscillating in the Y direction with the same amplitude and different phases. The trajectories of their centers in the X,Y plane differ as to the direction of the approach to, and the minimum distance from, the conical intersection. In all three cases, A, B and C, however, the initial wave packet has the same total energy.

We have run QM, VM, and TSH simulations. In case A, the VM-LZ approximation is also viable. In the full QM and in the VM treatments the initial conditions B and C are specified by the corresponding superposition of $|1,v\rangle$ states. In the TSH

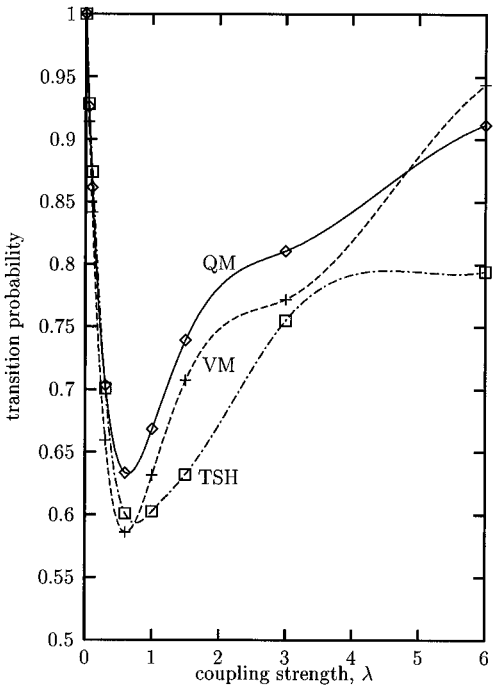

Figure 8. Transition probability from the upper to the lower adiabatic surface, $P_{u\to l}$, for the 2D model. The initial Gaussian wave packet is endowed with a non vanishing average momentum along the Y coordinate (case C, section 3.B).

procedure, we sample the initial coordinates and velocities so as to reproduce the wanted quantal distributions. The transition probabilities $P_{u\to l}$ are shown in Figures 6−8. They are generally lower than those obtained when starting with $v = 0$: qualitatively, hitting the conical intersection centrally and with the most concentrated wave packet yields the most diabatic behavior. In all cases the VM results are quite close to the QM ones. The agreement of TSH with QM improves in all cases A, B and C, with respect to what was found in the previous section. Overall, we take these results as an indication that the stationary $v = 0$ initial conditions are probably the most severe benchmark for TSH calculations, and generally better performances of this method can be expected in different situations.

4. Results of 3D and 4D Calculations

Three- and four-dimensional models were set up, in order to ascertain the cooperative or competitive effects of two or three coupling coordinates. The model electronic Hamiltonian $\mathbf{H}(X,Y_1...Y_N)$, with $N = 2$ or 3, is quite analogous to the 2D one presented in section 2:

$$H_{11} = D_1 e^{-\alpha_1(X+X_1)} + \sum_{\alpha}^{N} \frac{1}{2} K_\alpha Y_\alpha^{\,2} \tag{17}$$

$$H_{22} = D_2[e^{-2\alpha_2(X-X_2)} - 2e^{-\alpha_2(X-X_2)}] + \sum_{\alpha}^{N} \frac{1}{2} K_\alpha Y_\alpha^{\,2} + \Delta$$

$$H_{12} = \sum_{\alpha}^{N} \gamma_\alpha Y_\alpha e^{-\beta_1(X-X_3)^2} e^{-\beta_2 Y_\alpha^{\,2}}$$

All the parameters are the same as before, including $K_1 = K = 0.09$ au, with the addition of $K_2 = 0.10$ au and $K_3 = 0.1125$ au. The reduced masses M_α for the Y_α coordinates are 10 000, 9000, and 8000 au, respectively. These values were chosen so as to obtain slightly different vibrational frequencies ($\omega_\alpha = 658$, 732, and 823 cm^{-1}, respectively) for the coupling modes, without altering the widths $\Delta Y_\alpha = (2M_\alpha\omega_\alpha)^{-1/2}$ which appear in the

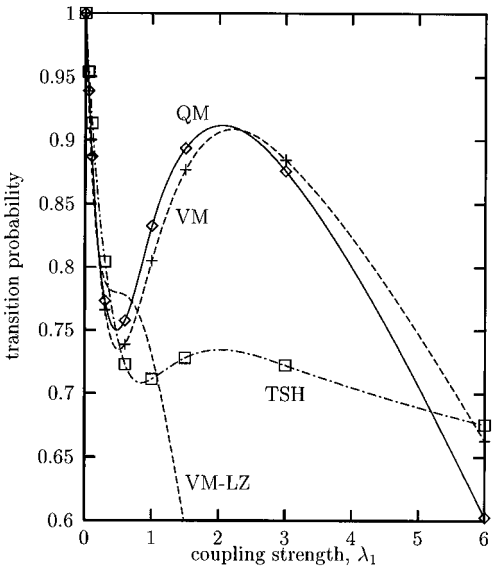

Figure 9. Transition probability from the upper to the lower adiabatic surface, $P_{u\to l}$, for the 3D model with two equal couplings (3D-e), $\lambda_1 = \lambda_2$.

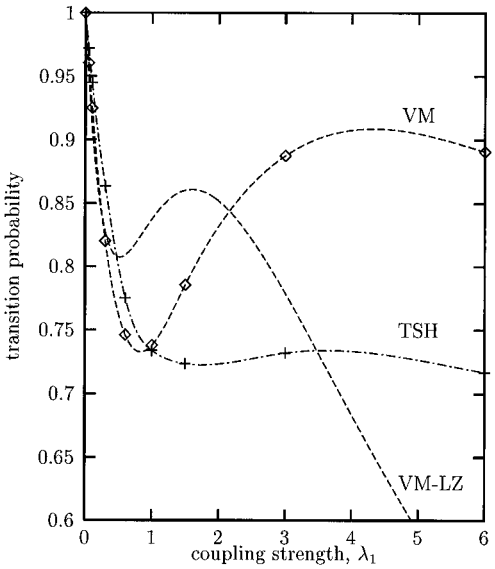

Figure 10. Transition probability from the upper to the lower adiabatic surface, $P_{u\to l}$, for the 3D model with two unequal couplings (3D-u), $\lambda_1 = 4\lambda_2$.

definition of the λ parameter. The QM, VM, and VM-LZ treatments are as described in section 2, except that the wave function expansions (4) and (8) are made on two- or three-mode vibrational bases, therefore with two or three quantum numbers v_α.

The γ_α factors are varied in order to investigate different coupling schemes. In the 3D-e model, we have two coupling coordinates with $\gamma_1 = \gamma_2$. In the 3D-u model, the two couplings are different, $\gamma_1 = 2\gamma_2$. Similarly, the 4D-e and 4D-u models are characterized by three couplings, respectively $\gamma_1 = \gamma_2 = \gamma_3$ and $\gamma_1 = 2\gamma_2 = 2\gamma_3$. The results of the simulations, all expressed as functions of $\lambda_1 = 2\pi\Delta Y^2\gamma_1^2/\dot{X}F_x$, are shown in Figures 9−11. For the 3D-e model we have also run full QM calculations and found that the VM results are again very good approximations of the exact ones. Therefore, for the other cases, only the VM results are given. Notice that, on the contrary, the Landau−Zener approximate solution breaks down in the 3D and 4D cases, because of the presence of very close lying avoided crossings. The TSH results show the same trends as in the 2D case.

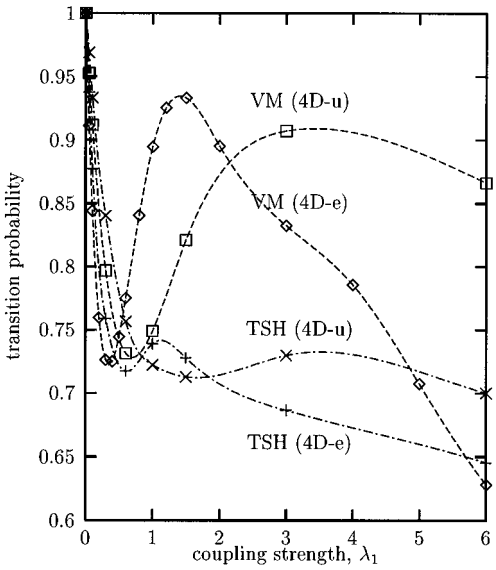

Figure 11. Transition probability from the upper to the lower adiabatic surface, $P_{u\to l}$, for the 4D models with three equal couplings $\lambda_1 = \lambda_2 = \lambda_3$ (4D-e), and with three unequal couplings $\lambda_1 = 4\lambda_2 = 4\lambda_3$ (4D-u).

Generally speaking, summing up more couplings increases the overall effect, in the sense that the $P_{u\to l}(\lambda_1)$ functions are displaced toward lower λ values. This effect increases in the order 3D-u < 4D-u < 3D-e < 4D-e. A better analysis of these findings can be done by identifying two special coordinates for each conical intersection:[25] one coincides with the gradient of $H_{11}-H_{22}$; the other one with that of H_{12}. In our models, the former coordinate is always X; the latter (the coupling coordinate) is

$$Y_c = (\sum_{\alpha=1}^{N}\gamma_\alpha^2)^{-1/2}(\sum_{\alpha=1}^{N}\gamma_\alpha Y_\alpha) \tag{18}$$

Starting from an intersection point, a displacement in any direction Z, orthogonal to these two coordinates, leaves the **H** matrix unchanged, except for a common shift of the diagonal matrix elements. Therefore, the Z coordinates do not couple the diabatic states, nor the adiabatic ones. We shall characterize a conical intersection by the coupling factor related with the Y_c coordinate:

$$\gamma_c = \frac{\partial H_{12}}{\partial Y_c} = (\sum_{\alpha=1}^{N}\gamma_\alpha^2)^{1/2} \tag{19}$$

The width of the wave packet in the Y_c dimension is

$$\Delta Y_c = (\sum_{\alpha=1}^{N}\gamma_\alpha^2)^{-1}(\sum_{\alpha=1}^{N}\gamma_\alpha^2\Delta Y_\alpha^2)^{1/2} \tag{20}$$

(that is, because with our choice of the parameters all ΔY_α are equal, $\Delta Y_c = \Delta Y_\alpha$). Then, an effective coupling strength can be defined as

$$\lambda_e = \frac{2\pi\Delta Y_c^2\gamma_c^2}{\dot{X}F_x} \tag{21}$$

In Figure 12 we show the $P^{(VM)}$ probabilities for all the 2D, 3D, and 4D models, as functions of λ_e. All the curves follow the same trend, and the quantitative agreement is good up to rather strong couplings. This means that the wave packet dynamics in the presence of a multidimensional conical intersection can be analyzed in terms of a single coupling

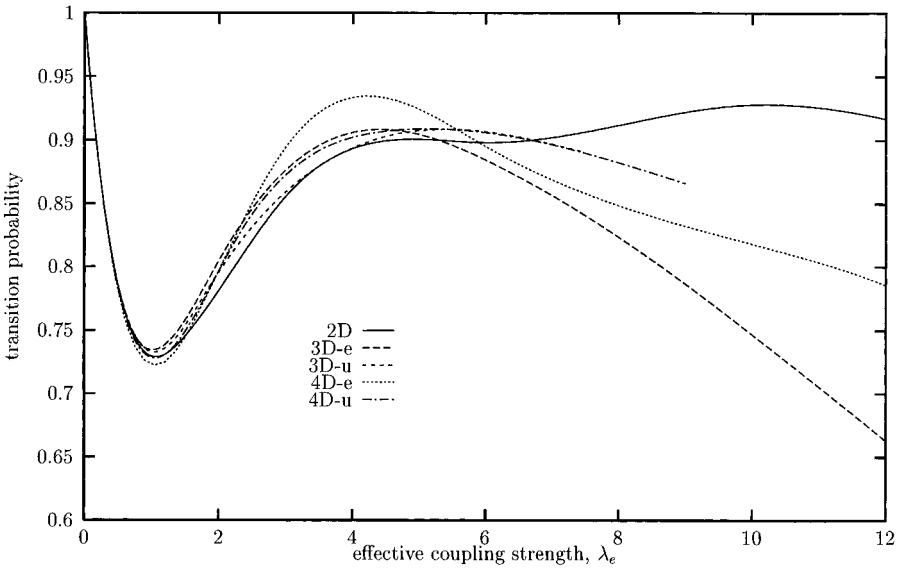

Figure 12. Transition probability from the upper to the lower adiabatic surface, $P_{u\to l}$, versus the effective coupling parameter λ_e. VM results for all the 2D, 3D, and 4D models.

coordinate, and the essential information is contained in the effective coupling parameter λ_e. Notice that a reduction of the Jahn−Teller problem from multimode to one-mode was already achieved by Cederbaum *et al*.,[26,27] in the same spirit as the preceding discussion.

5. Conclusions

We have set up a model of a conical intersection and studied the dynamics of a wave packet that travels along a symmetric coordinate and is stationary, or makes small amplitude oscillations, along the coupling coordinates. The expansion of the wave packet in a basis of vibrational eigenfunctions for the coupling modes allows one to understand at least qualitatively the variation of the transition probability from the upper to the lower electronic hypersurface as a function of the coupling strength. A single effective coupling parameter can be defined for each physical situation, even in the presence of more than one coupling coordinate, in analogy with the Massey parameter for avoided crossings:[28] this is a first step toward a classification of multidimensional conical intersections in terms of their dynamical properties. The determination of potential energy surfaces and couplings lies within the scope of electronic structure calculations. The connection with experimental results needs accurate treatments of the vibronic dynamics. However, our model indicates what can be qualitatively expected in typical situations: namely, strong vibrational excitation in the antisymmetric modes of the products, when large electronic couplings give place to conical intersections with steep sides.

Classical trajectories plus surface hopping correctly reproduce the quantum mechanical results for weak couplings, but larger deviations are found in the strong coupling regime. Better results are obtained when the initial wave packet contains some vibrational excitation in the coupling mode. As already discussed in a previous paper,[18] there are strong indications that the semiclassical treatment of transitions induced by the motion along the antisymmetric coordinate is flawed, at least for a zero-point vibrational wave function. Therefore we have tested a mixed treatment, classical for the symmetric coordinate and quantum mechanical for the coupling modes: the results are in very good agreement with the full quantum mechanical ones, with a much reduced computational effort.

Future work should extend this investigation to different geometries of approach of the wave packet to the conical intersection, including for instance a large amplitude motion along the antisymmetric coordinate.

Acknowledgment. This work was partially supported by the C. N. R. through the grant "Dynamics, reactivity and structure of molecular solutes". We are grateful to the authors of the TEMPO package, J. Broeckhove, B. Feyen, and P. Van Leuven, for supplying us with a copy of the program, and to G. Granucci for very helpful discussions.

References and Notes

(1) Michl, J.; Bonačić-Koutecký, V. *Electronic Aspects of Organic Photochemistry*; Wiley: New York, 1990.
(2) Desouter-Lecomte, M.; Sannen, C.; Lorquet, J. C. *J. Chem. Phys.* **1983**, *79*, 894.
(3) Mielke, S. L.; Tawa, G. J.; Truhlar, D. G.; Schwenke, D. W. *J. Am. Chem. Soc.* **1993**, *115*, 6436.
(4) Stock, G.; Domcke, W. *J. Phys. Chem.* **1993**, *97*, 12466.
(5) Müller, H.; Köppel, H.; Cederbaum, L. S. *J. Chem. Phys.* **1994**, *107*, 10263.
(6) Dixon, R. N. *Chem. Soc. Rev.* **1994**, 375.
(7) Klessinger, M. *Angew. Chem., Int. Ed. Engl.* **1995**, *34*, 549.
(8) Kuppermann, A. In *Dynamics of Molecules and Chemical Reactions*; Wyatt, R. E., Zhang, J. Z., Eds.; Dekker: New York, 1996; p 411.
(9) Dixon, R. N. *Mol. Phys.* **1996**, *88*, 949.
(10) Bearpark, M. J.; Bernardi, F.; Clifford, S.; Olivucci, M.; Robb, M. A.; Smith, B. R. *J. Am. Chem. Soc.* **1996**, *118*, 169.
(11) Clifford, S.; Bearpark, M. J.; Bernardi, F.; Olivucci, M.; Robb, M. A.; Smith, B. R. *J. Am. Chem. Soc.* **1996**, *118*, 7353.
(12) Worth, G. A.; Meyer, H.-D.; Cederbaum, L. S. *J. Chem. Phys.* **1996**, *105*, 4412.
(13) Tully, J. C. *J. Chem. Phys.* **1990**, *93*, 1061.
(14) Tully, J. C. *Int. J. Quantum Chem. Symp.* **1991**, *25*, 299.
(15) Gislason, E. A. *Adv. Chem. Phys.* **1992**, *82*, part 2, 321.
(16) Chapman, S. *Adv. Chem. Phys.* **1992**, *82*, part 2, 423.
(17) Smith, B. R.; Bearpark, M. J.; Robb, M. A.; Bernardi, F.; Olivucci, M. *Chem. Phys. Lett.* **1995**, *242*, 27.
(18) Ferretti, A.; Granucci, G.; Lami, A.; Persico, M.; Villani, G. *J. Chem. Phys.* **1996**, *104*, 5517.
(19) Manthe, U.; Köppel, H. *J. Chem. Phys.* **1990**, *93*, 1658.
(20) Seidner, L.; Domcke, W. *Chem. Phys.* **1994**, *186*, 27.
(21) Ferretti, A.; Lami, A.; Villani, G. *J. Chem. Phys.* **1997**, *106*, 934.
(22) Cimiraglia, R.; Persico, M.; Tomasi, J. *Chem. Phys.* **1978**, *34*, 103.
(23) Broeckhove, J.; Feyen, B.; Lathouwers, L.; Arickx, F.; Van Leuven, P. *Chem. Phys. Lett.* **1990**, *174*, 504.
(24) Cattaneo, P.; Persico, M. Unpublished results.
(25) Atchity, G. J.; Xanteas, S. S.; Ruedenberg, K. *J. Chem. Phys.* **1991**, *95*, 1862.
(26) Cederbaum, L. S.; Haller, E.; Domcke, W. *Solid State Commun.* **1980**, *35*, 879.
(27) Haller, E.; Cederbaum, L. S.; Domcke, W. *Mol. Phys.* **1980**, *41*, 1291.
(28) Desouter-Lecomte, M.; Leyh-Nihant, B.; Praet, M. T.; Lorquet, J. C. *J. Chem. Phys.* **1987**, *86*, 7025.
(29) Hase, W. L.; Duchovic, R. J.; Hu, X.; Lim, K. F.; Lu, D.-H.; Swamy, K. N.; Vande Linde, S. R.; Wolf, R. J. *VENUS. Quantum Chemistry Program Exchange* **1996**, *16*, 43.